0026-895X/10/7701-26–34$20.00
MOLECULAR PHARMACOLOGY
Vol. 77, No. 1
58750/3546611
Mol Pharmacol 77:26–34, 2010
Printed in U.S.A.

Inhibitors of the Mitochondrial Citrate Transport Protein: Validation of the Role of Substrate Binding Residues and Discovery of the First Purely Competitive Inhibitor[S]

Sreevidya Aluvila, Jiakang Sun, David H. T. Harrison, D. Eric Walters, and Ronald S. Kaplan

Department of Biochemistry and Molecular Biology, Chicago Medical School, Rosalind Franklin University of Medicine and Science, North Chicago, Illinois

Received June 22, 2009; accepted October 20, 2009

ABSTRACT

The mitochondrial citrate transport protein (CTP) is critical to energy metabolism in eukaryotic cells. We demonstrate that 1,2,3-benzenetricarboxylate (BTC), the classic and defining inhibitor of the mitochondrial CTP, is a mixed inhibitor of the reconstituted Cys-less CTP, with a strong competitive component [i.e., a competitive inhibition constant (K_{ic}) of 0.12 ± 0.02 mM and an uncompetitive inhibition constant (K_{iu}) of 3.04 ± 0.74 mM]. Based on docking calculations, a model for BTC binding has been developed. We then determined the K_{ic} values for each of the eight substrate binding site cysteine substitution mutants and observed increases of 62- to 261-fold relative to the Cys-less control, thereby substantiating the importance of each of these residues in BTC binding. It is noteworthy that we observed parallel increases in the K_m for citrate transport with each of these binding site mutants, thereby confirming that with these CTP variants, K_m approximates the K_d (for citrate) and is therefore a measure of substrate affinity. To further substantiate the importance of these binding site residues, in silico screening of a database of commercially available compounds has led to discovery of the first purely competitive inhibitor of the CTP. Docking calculations indicate that this inhibitor spans and binds to both substrate sites simultaneously. Finally, we propose a kinetic model for citrate transport in which the citrate molecule *sequentially* binds to the external and internal binding sites (per CTP monomer) before transport.

Citrate is a key intermediate at the intersection of carbohydrate and lipid metabolism. Within the mitochondrion, it is part of the tricarboxylic acid (Krebs) cycle; in the cytoplasm, it can be broken down to acetyl CoA to support fatty acid, lipid, and cholesterol biosyntheses (Spencer and Lowenstein, 1962; Srere and Bhaduri, 1962; Greville, 1969; Watson and Lowenstein, 1970). The mitochondrial citrate transport protein (CTP) is an obligate antiporter that mediates the exchange of the dibasic form of tricarboxylic acids (e.g., citrate or isocitrate) either for each other in yeast (Kaplan et al., 1995; Xu et al., 2000) or for dicarboxylic acids (e.g., malate, succinate) or phosphoenolpyruvate in higher eukaryotes (Robinson et al., 1971a,b; Palmieri et al., 1972).

Studies of the structure and function of membrane transporters are greatly facilitated by the availability of potent and specific inhibitors. In the case of the mitochondrial ADP/ATP carrier, which is a member of the same family of transport proteins as the CTP, inclusion of an inhibitor facilitated crystallization and subsequent determination of X-ray crystallographic structure (Pebay-Peyroula et al., 2003). However, for the CTP, only a few such inhibitors are known, and their potency is quite low. The best inhibitor available, 1,2,3-benzenetricarboxylate (BTC), was reported to be a competitive inhibitor, with K_i values ranging from 0.07 to 0.16 mM, and IC_{50} values of 3 to 8 mM (Robinson, 1971; Robinson et al., 1971a,b; Palmieri et al., 1972; Bisaccia et al., 1990). It should be noted that 1) none of these studies was conducted with the yeast mitochondrial CTP (i.e., the subject of the present investigations) and 2) the data that led investigators to conclude a competitive model for BTC inhibition often were not shown (Palmieri et al., 1972; Bisaccia et al., 1990).

We have previously used homology modeling to produce a model of the mitochondrial CTP (Walters and Kaplan,

This work was supported by the National Institutes of Health National Institute of General Medical Sciences [Grant GM054642].

Article, publication date, and citation information can be found at http://molpharm.aspetjournals.org.

doi:10.1124/mol.109.058750.

[S] The online version of this article (available at http://molpharm.aspetjournals.org) contains supplemental material.

ABBREVIATIONS: CTP, citrate transport protein; BTC, 1,2,3-benzenetricarboxylate; ZINC compound 792949, 4-chloro-3-[(3-nitrophenyl)sulfamoyl]benzoic acid; DMSO, dimethyl sulfoxide.

2004). Using a combination of docking calculations and analysis of the transport kinetics of single point mutations, we have identified two substrate binding sites in this transporter in its cytosolic-facing conformation (Ma et al., 2007) as depicted in Fig. 1. Here, we describe a number of studies of CTP inhibition. First, we examined the kinetic mechanism of the BTC-mediated inhibition of the yeast mitochondrial Cys-less CTP and found that BTC is a mixed inhibitor with a strong competitive component that affects not only the apparent Michaelis constant (K_m) for citrate, but also the apparent maximal transport velocity (V_{max}), albeit to a substantially lesser degree. Second, we have measured the competitive binding constant of BTC with previously described (Ma et al., 2007) single point variants of the substrate binding site residues. The results from these studies verify our previous contention that K_m is for the most part related to the K_d for citrate in these variants. Finally, we have used our homology model in a high throughput in silico screen of the ZINC database of commercially available compounds (Irwin and Shoichet, 2005; http://zinc.docking.org), and we have identified a competitive inhibitor that displays a slightly higher affinity for the CTP than that of BTC. It is noteworthy that, in contrast to BTC or citrate, the size, shape, and hydrogen bonding potential of the newly identified inhibitor suggests that it simultaneously spans both of the previously identified citrate binding sites. These results are combined to present a kinetic model for the CTP transport cycle.

Materials and Methods

Construction, Overexpression, Isolation, and Incorporation of Cys-Less and Single-Cys CTP Variants into Liposomal Vesicles. Single-Cys CTP mutants were constructed using the QuikChange site-directed mutagenesis kit (Stratagene, La Jolla, CA) as described previously (Ma et al., 2004). The Cys-less yeast mitochondrial CTP gene in pET-21a(+) was used as the starting template (Xu et al., 2000). Mutations were confirmed by sequencing both strands of the entire CTP open reading frame. BL21(DE3) growth and induction of CTP expression with isopropyl β-D-thiogalactoside were conducted as previously detailed (Kaplan et al., 1995; Xu et al., 1995). Two hours after induction, cells were harvested and lysed, and the inclusion body fraction was purified by centrifugation in a sucrose gradient (Kaplan et al., 1995; Xu et al., 1995). CTP mutants were then solubilized from the inclusion body pellet with 6 ml of ice-cold 1.2% (w/v) sarkosyl. After centrifugation at 314,000*g* for 45 min, the supernatant contained a given solubilized CTP mutant. Each mutant was then incorporated into liposomal vesicles, in the presence of 48 to 75 mM citrate, via the freeze-thaw sonication procedure as described previously (Kaplan et al., 1990, 1995). Except for the Cys-less CTP, all other single-Cys mutants were reconstituted with 75 mM citrate inside the liposome. Immediately before the transport assay, a given sample was thawed and sonicated on ice, and the extraliposomal citrate was removed via chromatography on a Dowex column (Ma et al., 2007). The sample was immediately assayed for transport. Protein was quantified via the method of Kaplan and Pedersen (1985).

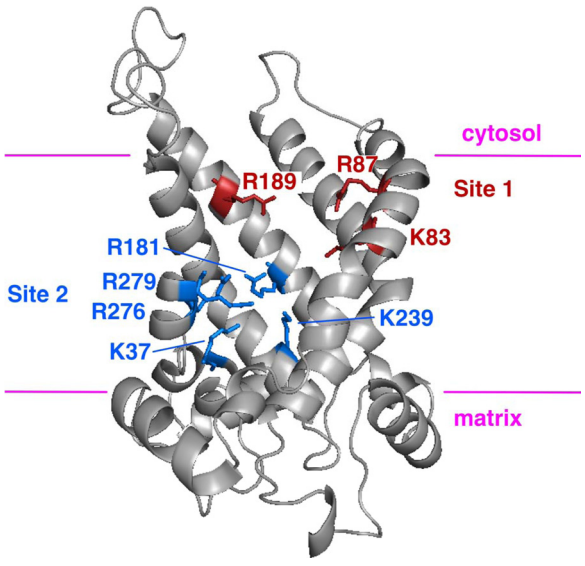

Fig. 1. Ribbon diagram of the homology modeled CTP structure in the cytosolic-facing conformation. Portions of helix I and helix VI have been removed for clarity. Key residues of citrate binding sites 1 and 2 are shown as stick structures in red and blue, respectively. The approximate boundaries of the mitochondrial inner membrane are shown as magenta lines.

Characterization of the Type of Inhibition of the Cys-Less CTP Mediated by BTC and the ZINC Compound 792949 and Determination of Inhibition Constants. We routinely work with a Cys-less form of the yeast mitochondrial CTP that displays native-like functional properties (Xu et al., 2000). The type of inhibition of the Cys-less CTP mediated by BTC and ZINC compound 792949 and the inhibition constants were determined as follows. Proteoliposomes (585 μl) were incubated with 45 μl of either buffer (experimental incubation) or BTC (Sigma Aldrich, St. Louis, MO) (control incubation) for 10 min at 21°C. Transport reactions (13–50 s) were then triggered by adding 49 μl of the above reaction mix to 25 μl of [1,5-^{14}C]citrate (0.05–14 mM; specific radioactivity, 43–430 × 10^2 cpm/nmol; GE Healthcare, Chalfont St. Giles, Buckinghamshire, UK) plus varying concentrations of BTC (0–1.5 mM; Sigma Aldrich) or varying concentrations of compound 792949 (0–2 mM; ChemBridge, San Diego, CA). Experimental incubations were quenched by the addition of 3.5 μl of 200 mM BTC, whereas control incubations received an equal volume of buffer. All transport incubations contained a final concentration of 9 mM BTC. After transport, intraliposomal radiolabeled citrate was separated from the external radiolabel via chromatography on 2.6 ml of Dowex resin in support columns (Bio-Rad Laboratories, Hercules, CA). The eluted intraliposomal radiolabel was quantified via liquid scintillation counting. The BTC-sensitive transport rate was calculated by subtracting the control value from the experimental value.

The data were then analyzed via Global fit analysis and Lineweaver-Burk ($1/v$ versus $1/S$) plots, in which v corresponds to the rate of a given transport reaction. In the case of BTC inhibition, both the K_{ic} (the competitive inhibition constant) and K_{iu} (the uncompetitive inhibition constant) values were calculated using the Global Fit method in the Prism program (ver. 4; GraphPad Software, San Diego, CA). In this method, the observed rate versus [S] data (in the presence and absence of inhibitors) can be fitted simultaneously according to the full nonlinear expression for mixed inhibition $v = V_{max}[S]/(K_m(1 + [I]/K_{ic}) + [S](1 + [I]/K_{iu}))$ (Cortés et al., 2001). But in the case of ZINC compound 792949 inhibition, the K_{ic} value was calculated using the global fit method using the nonlinear expression for competitive inhibition $v = V_{max}[S]/(K_m(1 + [I]/K_{ic}) + [S])$.

Modeling and In Silico Screening of Potential Inhibitors. High throughput in silico screening was carried out using version 5 of the DOCK software package (Shoichet et al., 1992; http://dock.compbio.ucsf.edu/). The following residues of the mitochondrial citrate transporter were previously identified as key components of substrate binding sites (Ma et al., 2007) and were used to define the target site for the DOCK calculations: lysine 83 and arginines 87 and 189 from site 1, and lysines 37 and 239 and arginines 181, 276, and 279 from site 2.

The ZINC database comprises millions of commercially available compounds. We prescreened the database, as follows. First, we ex-

cluded compounds with a calculated partition coefficient above 5.0, because these tend to have poor water solubility. We also excluded compounds with molecular mass over 500, because larger molecules are less likely to fit into citrate binding sites. Finally, we considered only compounds that have net charge of 0, −1, −2, or −3, because the transport pathway has an excess of positively charged side chains.

The output of the initial DOCK screening is a set of the 500 best-scoring compounds, docked into the modeled protein. From the initial set of 500 hits, we purchased and tested 30 compounds. These were selected as follows. First, we visually inspected each hit as it was placed in the transporter model by the DOCK program. We discarded compounds that did not make at least three favorable interactions with the protein that were well separated spatially. Next, we observed that many of the hits could be grouped into clusters having common core structures; we chose the best fitting 1 or 2 analogs for each cluster to have as much diversity as possible in our test set.

Testing of these 30 compounds identified four compounds with inhibitory activity (i.e., ≥50% inhibition at a concentration of 1 mM). These four compounds were used as the basis for a similarity search of the ZINC database, to identify a second set of 13 compounds for testing. We identified two actives in this group that were then used for another round of similarity searching, and an additional 16 compounds were identified and tested and resulted in four actives. Thus, in total, 10 active compounds were identified. Similarity searching was carried out using the Cactvs algorithm (Ihlenfeldt et al., 2002) to calculate a Tanimoto similarity score; compounds with greater than 80% Tanimoto similarity were considered for testing.

Both BTC and the most potent inhibitor discovered by screening (i.e., compound 792949) were docked into the modeled transporter, and positions were optimized by side chain rotation and energy minimization, using the Molecular Operating Environment software, version 2008.10 (Chemical Computing Group, Montreal, QC, Canada).

Inhibition of the Cys-Less CTP by Compounds Identified from the ZINC Database. The inhibition of the Cys-less CTP by BTC and potential ZINC inhibitors was characterized as follows. Proteoliposomes (48 μl) were preincubated with 3.5 μl of either buffer (experimental sample) or 200 mM BTC (control sample) for 12 min at 21°C and were then further incubated with 0.5 μl of dimethyl sulfoxide (DMSO) or buffer or varying concentrations of BTC (0.05–5.5 mM) or potential ZINC inhibitors (0.1 μM–1 mM) for 12 min. The ZINC inhibitors were prepared freshly each day in DMSO (mostly) or buffer. Transport was initiated by the addition of 21.5 μl of 3.6 mM [1,5-^{14}C]citrate (specific radioactivity, 24 × 10^3 cpm/nmol; GE Healthcare), and the uptake time was 25 s. Experimental samples were quenched by the addition of 3.5 μl of 200 mM BTC, whereas the control samples received an equal volume of buffer. After transport, intraliposomal radiolabeled citrate was separated from the external radiolabel via chromatography on short (i.e., 4 cm) Dowex columns in Pasteur pipettes. The eluted intraliposomal radiolabel was quantified via liquid scintillation counting. The BTC- sensitive transport rate was calculated by subtracting the control value from the experimental value. The effect of BTC or a given inhibitor compound on citrate transport is expressed as the percentage inhibition of the initial BTC-sensitive citrate uptake (measured in the presence of buffer or DMSO). This was calculated by: 1) determining the BTC-sensitive transport rate via subtraction of the control value from the experimental value, in the absence of the inhibitor; 2) subtracting the control value from the experimental value obtained in the presence of varying concentrations of the inhibitor; 3) determining the ratio of this difference to the uninhibited BTC-sensitive citrate transport rate; and 4) application of the formula (1 − ratio) × 100.

Determination of the Kinetic Parameters of CTP Variants. The kinetic parameters (K_m and V_{max}) of the Cys-less and the single-Cys CTP variants were determined as follows. Proteoliposomes (45 μl) were preincubated with 5 to 7 μl of either buffer (experimental sample) or 1 M BTC (control sample) for 10 to 12 min and were then further incubated with or without 2 μl of deionized/distilled water for an additional 10 to 12 min. The transport reaction was triggered via the addition of 21.5 μl of varying concentrations of [1,5-^{14}C]citrate (0.05–75 mM; specific radioactivity, 28–220 × 10^2 cpm/nmol; GE Healthcare). To enable construction of a stock solution with increased specific radioactivity, the [^{14}C]citrate source had been concentrated approximately 22-fold by evaporation under vacuum. After transport incubations that ranged from 13 s to 2.75 h (depending on the intrinsic activity of a given CTP mutant), the experimental sample was quenched by the addition of 5 to 7 μl of 1 M BTC. The control sample received an equal volume of buffer. Transport reactions were conducted at room temperature (21°C). All transport incubations contained a final concentration of 75 mM BTC. Intraliposomal radiolabeled citrate was then separated from the external radiolabel via chromatography on 2.6 ml of Dowex resin in Bio-Rad support columns. The eluted (i.e., intraliposomal) radiolabel was quantified via liquid scintillation counting. It is noteworthy that a much higher level of BTC was used in these experiments than previously (i.e., 75 mM, versus 9 mM in Ma et al., 2007) to more completely quench the transport reaction catalyzed by the single-Cys substitution mutations. In addition, an increased quantity of Dowex resin was used to ensure efficient capture of all extraliposomal citrate even at the high substrate concentrations employed. In combination, these changes resulted in a more accurate determination of the K_m and V_{max} values of the CTP binding site mutants (Supplemental Fig. 1) than previously reported (Ma et al., 2007). The BTC-sensitive transport rate was then calculated by subtracting the control value from the experimental value. The rate of uptake versus substrate concentration curves were fitted to the Michaelis-Menten equation $v = V_{max} \cdot S/(K_m + S)$, using a nonlinear least-squares curve fit in GraphPad Prism. The final K_m and V_{max} values for each single-Cys CTP mutant were calculated by taking the mean of the best fit K_m and V_{max} values derived from each separate v-versus-S profile.

Determining the K_{ic} of the Cysteine Substitution Substrate Binding Site Mutants for BTC. The competitive inhibition constant (K_{ic}) of the substrate binding site mutants of CTP was determined as follows. Proteoliposomes (585 μl) were incubated with 91 μl of either buffer (experimental incubation) or BTC (control incubation) for 10 min at 21°C. Transport reactions (5–225 min) were then triggered by adding 52 μl of the above reaction mix to 26 μl of [1,5-^{14}C] citrate (0.1–25 mM; specific radioactivity, 25–2370 × 10^2 cpm/nmol) plus water or varying concentrations of BTC (0–50 mM). It should be noted that before the transport experiments, the [^{14}C]citrate source had been concentrated approximately 22-fold by evaporation under vacuum to enable construction of a stock solution with increased specific radioactivity. Experimental incubations were quenched by the addition of 7 μl of 780 mM BTC, whereas control incubations received an equal volume of buffer. Transport incubations contained a final concentration of 64 mM BTC. After transport, intraliposomal radiolabeled citrate was separated from the external radiolabel via chromatography on 2.6 ml of Dowex resin in Bio-Rad support columns. The eluted intraliposomal radiolabel was quantified via liquid scintillation counting. The BTC-sensitive transport rate was calculated by subtracting the control value from the experimental value.

The data were then analyzed as follows. Although it was possible to bracket the K_m for the binding site mutants in the absence of inhibitor, it was not practical to do so in the presence of the BTC inhibitor. At three relatively low concentrations of citrate (below K_m) for each variant, BTC was varied (i.e., at least nine concentrations of BTC were tested), and velocity data were obtained. For each mutant at each concentration of inhibitor, the reciprocal slope of a two- or three-point v-versus-S plot was recorded, fixing the x- and y-intercepts to zero. Where significant curvature was found, the high citrate concentration point was excluded from the slope analysis. From this reciprocal slope, K_m/V_{max} apparent was estimated and plotted against the BTC concentration (Supplemental Fig. 2). It can be

shown that the x-intercept from this second graph ($(K_m/V_{max})_{app}$ versus [BTC]) is equal to the competitive inhibition constant, K_{ic}.

Results

Characterization of the Kinetic Mechanism of the BTC-Mediated Inhibition of the Cys-Less CTP. BTC is considered the classic and defining inhibitor of the mitochondrial inner membrane CTP (Robinson et al., 1971a,b; Palmieri et al., 1972). In the present studies, we characterized the kinetic mechanism by which BTC inhibits the yeast mitochondrial Cys-less CTP after its overexpression in *Escherichia coli*, solubilization, and functional reconstitution in a well characterized liposomal system (Kaplan et al., 1990; Xu et al., 2000). BTC-mediated inhibition of the Cys-less CTP was examined by measuring the [^{14}C]citrate uptake rate in the presence of several different citrate and BTC concentrations. The data were analyzed via both a Lineweaver-Burk plot and a v-versus-S plot (Fig. 2). As depicted in Fig. 2A, the Lineweaver-Burk plot indicates that within the range of BTC concentrations tested, the K_m increases by more than 1200% and the V_{max} decreases by 24% as the concentration of BTC is increased from 0 to 1.5 mM. The observation that the plotted lines at increasing BTC levels intersect, but do not do so at either the x- or y-axes (Fig. 2A, inset), indicates that a mixed inhibition pattern is observed. This conclusion is further supported by our observation in Fig. 6C that a replot of the y-intercepts (i.e., $1/V_{max}$ values) depicted in Fig. 2A versus BTC concentration yields a line with a positive slope, thereby clearly indicating that BTC is not a purely competitive inhibitor. Thus, we conclude that BTC is a mixed inhibitor of the CTP, with a predominantly competitive component. This type of inhibition pattern is further supported by analysis of the data via the Dixon and the Cornish-Bowden plots (data not shown).

As depicted in Fig. 2B, the v-versus-S data were then analyzed via global fit analysis for mixed inhibition enabling calculation of both the K_{ic} (the competitive inhibition constant) and K_{iu} (the uncompetitive inhibition constant) values. The competitive inhibition constant K_{ic} is 0.12 ± 0.02 mM and the uncompetitive inhibition constant K_{iu} is 3.04 ± 0.74 mM. It is noteworthy that the K_{iu} is 25-fold higher than the K_{ic} value, confirming that BTC is primarily but not exclusively a competitive inhibitor of the Cys-less CTP.

Proposed Modes of BTC Binding to the CTP. Because the CTP transport path has numerous arginine and lysine side-chains, and BTC has three carboxylate groups, it is not surprising that there are numerous possible ways to dock BTC. We have previously identified two substrate binding sites in the CTP (Ma et al., 2007). When we carried out the computational docking of BTC to our model of the CTP structure, we observed a large cluster of docking poses with BTC in the second (deeper) substrate binding site, and a smaller cluster of docking poses with BTC in the first substrate binding site. Representative configurations are shown in Fig. 3. Figure 3A shows that ion pair interactions form between the BTC carboxylate groups and the side chains of Lys83, Arg87, and Arg189; all of these were previously identified as part of substrate binding site 1. As illustrated in Fig. 3B, the BTC carboxylates can interact with the side chains of Lys37, Lys134, Arg181, Lys239, and Arg276; all of these except Lys134 were previously identified as components of substrate binding site 2. It is noteworthy that we have previously hypothesized that Lys134 resides in close juxtaposition to site 2, such that it is capable of forming an ionic hydrogen bond to the C5-COO$^-$ of citrate (Ma et al., 2007).

Our proposed BTC binding modes garner further support by the experimental results depicted in Table 1. Because BTC is a mixed inhibitor of the Cys-less CTP with a strong competitive component (K_{ic} = 0.12 ± 0.02 mM and K_{iu} = 3.04 ± 0.74 mM) and because both citrate and BTC are structurally very similar (Supplemental Fig. 3B), we assume that the two ligands mainly bind to the CTP at the same sites. Consequently, if each of the substrate binding site residues plays a prominent role in binding BTC, then we would expect to observe an increase in the K_{ic} value for BTC with each of the binding site mutants when compared with the Cys-less CTP control. We tested this notion experimentally by measuring the [^{14}C]citrate transport rate in the presence of varying citrate and inhibitor concentrations. For each inhibitor concentration, v-versus-S data were used to

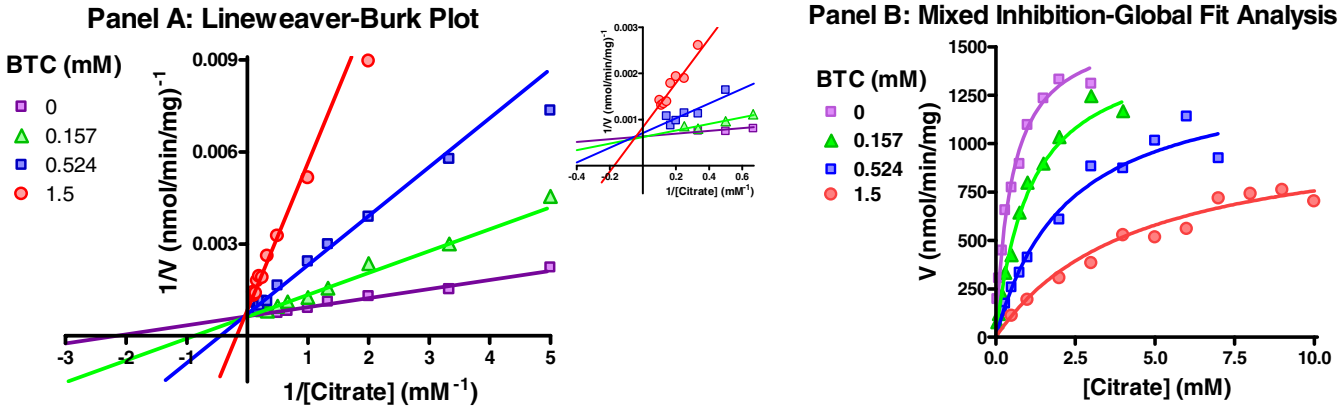

Fig. 2. Determination of kinetic mechanism and inhibition constants of BTC-mediated inhibition of the Cys-less CTP. A, Lineweaver-Burk plot depicting the effect of BTC on the citrate transport activity. The citrate/citrate exchange (0.1–10 mM external/48 mM internal) was determined in the absence (purple line) and in the presence of BTC (green line, 0.157 mM; blue line, 0.524 mM; and red line, 1.5 mM) as described under *Materials and Methods*. Nonlinear regression analysis of v-versus-[S] data was used to calculate V_{max} (apparent) and K_m (apparent) for each inhibitor concentration. These lines were then plotted on a double reciprocal plot. Inset shows the y-intercept ($1/V_{max}$) of each line. V_{max} (apparent) decreases, whereas K_m (apparent) increases with increasing concentration of the inhibitor BTC. B, global fit analysis of v-versus-[S] data (in the presence and absence of inhibitors) fitted simultaneously according to the full nonlinear expression for mixed inhibition.

calculate $(K_m/V_{max})_{apparent}$. Replots of $(K_m/V_{max})_{apparent}$ versus [Inhibitor] were constructed to determine the K_{ic} value of each mutant (note that the *x*-intercepts in these plots correspond to the K_{ic} value; see Supplemental Fig. 2). As depicted in Table 1, we observed a 62- to 261-fold increase in the K_{ic} values of the binding site mutants for BTC. Furthermore, because each of the single-Cys binding site mutants displayed a large increase in their apparent K_m values compared with the Cys-less control (i.e., 4- to 50-fold increases; see Table 1 and Supplemental Fig. 1), and a significant reduction in their V_{max} values and catalytic efficiencies (Supplemental Fig. 1) (Ma et al., 2007), we infer that with each of the binding site mutants, the k_2 (k_{cat}) for transport is severely depressed. Therefore, K_m approximates K_d. This hypothesis is consistent with the observation that the increases in the binding site single-Cys mutant K_{ic} values for BTC parallel the observed increases in the K_m values for these mutants, thereby supporting our contention that with these mutants the K_m values approximate the K_d values and therefore primarily reflects the affinity of the transporter for substrate.

Figure 4 displays the effect of a given binding site mutation on the relative binding energy (i.e., $\Delta\Delta G$) of CTP for BTC compared with that of the Cys-less CTP versus the effect of a given mutation on the K_m for citrate transport (i.e., log K'_m/K_m, where K'_m is the Michaelis constant for a given CTP

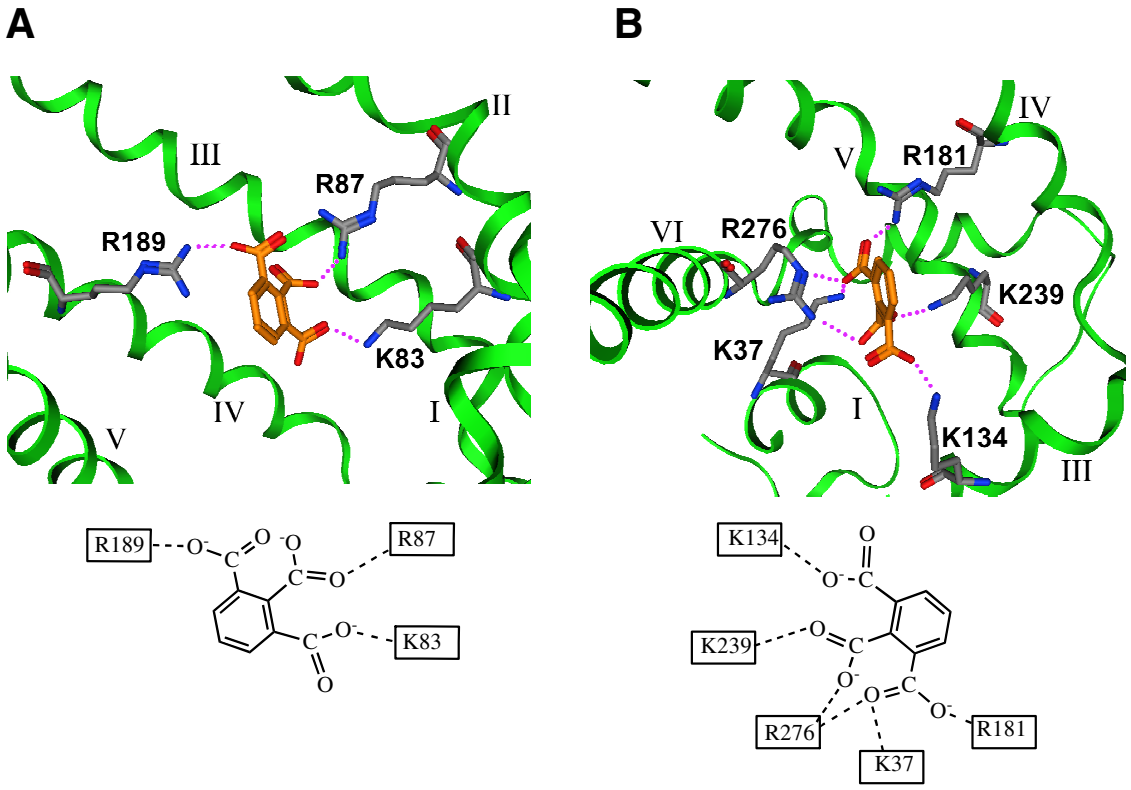

Fig. 3. Important binding interactions for the docked conformations of BTC with the mitochondrial CTP model. Top views, CTP backbone shown as green ribbon, with transmembrane domains identified using Roman numerals, with interacting side chains shown as stick structures colored by atom type and BTC shown as a stick structure with orange carbon atoms. Ion-pair interactions are shown using magenta dotted lines. Bottom, schematic representation with ion-pair interactions shown as dotted lines. A, binding of BTC in previously identified (Ma et al., 2007) citrate binding site 1. B, binding of BTC in citrate binding site 2. Portions of helix VI in A and helices I and II in B have been removed for clarity.

TABLE 1

Effect of cysteine substitution mutation of the CTP substrate binding site residues on the K_m for citrate transport and the K_{ic} (the competitive inhibition constant) of BTC binding to CTP

Transport reactions and calculations of K_m and K_{ic} were conducted as described under *Materials and Methods*. K_m values (± S.E.) were obtained from at least duplicate *v*-versus-[S] profiles employing at least 10 different substrate concentrations that bracketed the K_m value. K_{ic} values (± S.E.) were extracted from $(K_m/V_{max})_{app}$ versus [BTC] plots (see Supplemental Fig. 2).

Mutation	K_m	Increase in K_m Compared with Cys-Less	K_{ic} of BTC	Increase in K_{ic} Compared with Cys-Less
	mM	*-fold*	*mM*	*-fold*
Cys-less	0.62 ± 0.04		0.124 ± 0.015	
Substrate binding site 1				
K83C	28.2 ± 7.2	45	24.1 ± 3.7	194
R87C	31.1 ± 4.7	50	25.0 ± 4.6	202
R189C	14.5 ± 1.7	23	15.1 ± 2.2	122
Substrate binding site 2				
K37C	2.3 ± 0.6	4	7.7 ± 0.8	62
R181C	25.8 ± 5.2	42	15.9 ± 2.5	128
K239C	30.9 ± 10.9	50	13.2 ± 1.2	106
R276C	16.4 ± 3.3	26	32.4 ± 5.4	261
R279C	19.5 ± 5.4	31	18.6 ± 2.4	150

binding site mutant and K_m is the constant for the Cys-less control). Because binding energy is related to the log of the dissociation constant by the expression $\Delta G = -2.303 \cdot R \cdot T \cdot \log K$ (where R is the gas constant and T is absolute temperature) and because the individual binding energies between each binding site residue and a given ligand are expected to add to the total binding site free energy, one expects a constant relationship between the $\Delta\Delta G$ for BTC and the logarithm of the relative K_m for citrate if K_m in fact approximates K_d. As depicted in Fig. 4, we observed that six of the eight binding site mutants reside on the best fit line, thereby indicating a strong correlation between the binding energy of a particular residue for both BTC and citrate. We observe that binding site mutant R276C lies above the best fit line, indicating a greater than expected contribution of this residue to BTC binding, whereas one binding site mutant (i.e., K239C) lies to the right of the best fit line, suggesting a stronger than expected contribution of this residue to the K_m for citrate transport. It is noteworthy that each of these two residues is located within binding site 2. The observation that the Cys-less CTP resides significantly to the right of the line is readily explained by the contribution of k_{cat} toward the K_m value, in contrast to all of the single Cys binding site mutants that display k_{cat} values that are dramatically reduced.

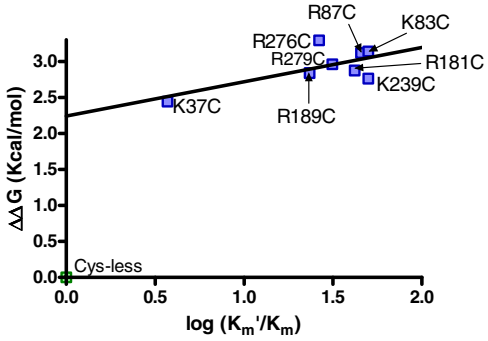

Fig. 4. Contribution of CTP binding site residues to the binding energy for BTC versus citrate. This figure plots the change in the free energy of BTC binding ($\Delta\Delta G$) of the single-Cys binding site mutants relative to the Cys-less control versus the log of the ratio of the corresponding K_m values for citrate transport. Data were extracted from Table 1.

Identification of New CTP Inhibitors. We next proceeded to identify new inhibitors of the CTP via in silico screening of the ZINC database, which, at the time of these studies, consisted of more than 3 million commercially available small molecules (see *Materials and Methods*). An initial set of 30 compounds were purchased and tested. This was followed by two additional rounds of searching the database for compounds similar to the initial sets of active inhibitors. In total, 59 compounds were experimentally tested for inhibition of citrate transport. Ten of these produced at least 50% inhibition when tested at 1 mM. For comparison, in this assay, BTC produced 79% inhibition at this concentration. The active inhibitors identified are shown in Fig. 5, along with their ZINC database identifier codes and their percentage inhibition at 1 mM. The most potent inhibitor, compound 792949, produced 85% inhibition of citrate transport.

Inhibition Mechanism of Compound 792949. We characterized the kinetic mechanism by which compound 792949 inhibits the yeast mitochondrial Cys-less CTP by measuring

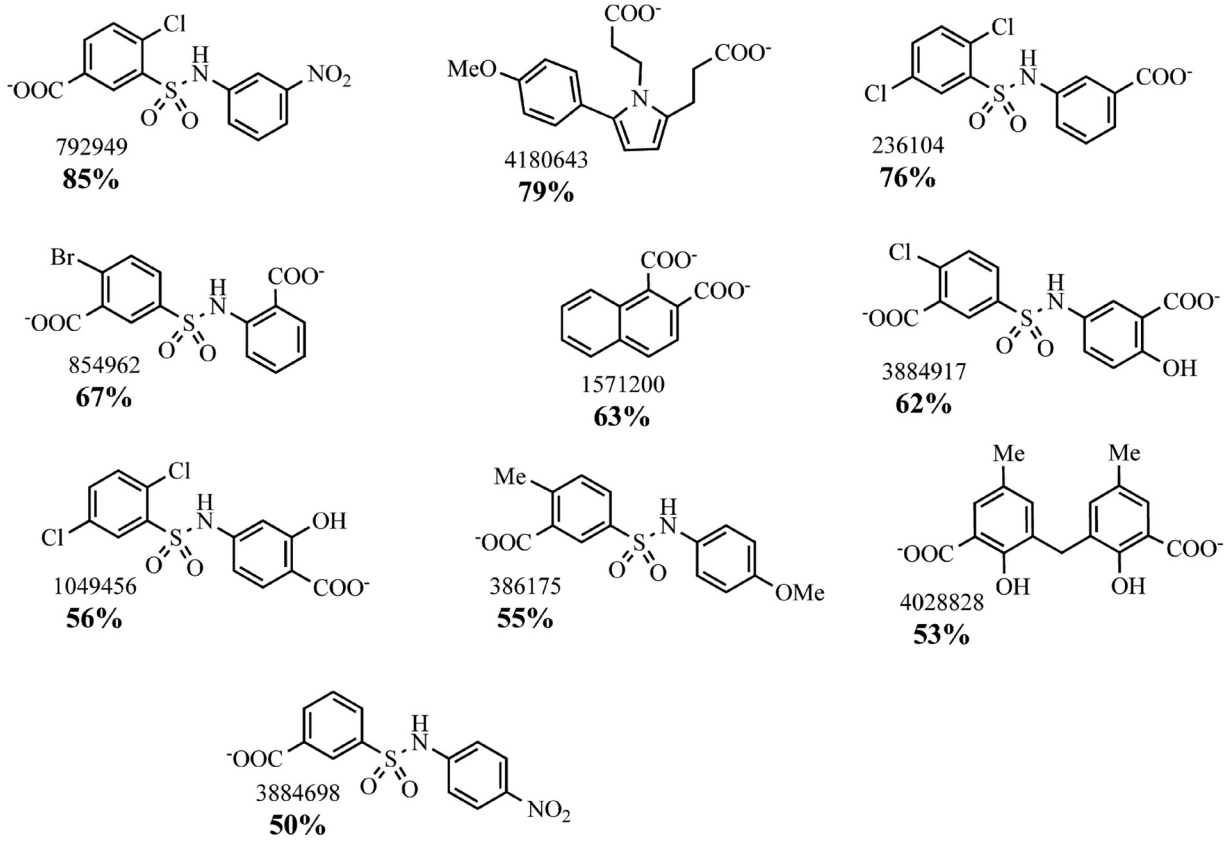

Fig. 5. Newly discovered inhibitors of the yeast mitochondrial citrate transporter. For each compound, the ZINC database ID number and the percentage inhibition at 1 mM concentration are listed.

the transport rate at a variety of different citrate and inhibitor concentrations. As depicted in Fig. 6, the data were analyzed via both a Lineweaver-Burk plot and a v-versus-S plot. The Lineweaver-Burk plot (A) indicates that within the range of inhibitor concentrations tested, the apparent K_m increases (38-fold), whereas no significant change in the apparent V_{max} was observed (Fig. 6, A, inset, and C, y-intercept replot). The observation that for 792949 the best-fit lines in Fig. 6A display essentially the same y-intercept is evidence of a purely competitive inhibitor. Based on a global fit analysis (Fig. 6B), the competitive inhibition constant K_{ic} is 0.048 ± 0.007 mM. It is noteworthy that, as depicted in Fig. 6C, a replot of the y-intercepts obtained in Fig. 6A as a function of the 792949 inhibitor concentration yields a line whose slope ($2.1 \pm 3.2 \times 10^{-5}$) does not significantly deviate from 0 (shown by the red dashed line), thus providing compelling graphical evidence that this inhibitor is purely competitive. For comparison, we also depict a replot of the data obtained with BTC (from Fig. 2A). In this case, it is evident that the slope of the re-plotted line ($14.2 \pm 1.8 \times 10^{-5}$) is nonzero, thus clearly indicating a mixed inhibition pattern.

Docking of compound 792949 into the CTP homology model (Fig. 7) produced a configuration in which the nitro group forms ionic hydrogen bonds with Lys83 and Arg87 of binding site 1, the sulfonamide group forms two ionic hydrogen bonds to Arg181 of binding site 2, and the carboxylate group forms ionic interactions with Lys37, Arg276, and Arg279 of binding site 2. In addition, the nitro-substituted ring has hydrophobic interaction with Leu120, and the chloro-substituted ring has hydrophobic interaction with Phe76 (not shown in Fig. 7). Thus, compound 792949 is capable of spanning portions of substrate binding sites 1 and 2, an observation in line with the fact that this inhibitor is approximately double the length of either citrate or BTC (Supplemental Fig. 3A).

Discussion

The present investigations characterize CTP inhibitors and their effects on the kinetics of substrate binding site cysteine substitution mutants and have resulted in several novel findings that are critical to understanding the mechanism of this metabolically important transporter.

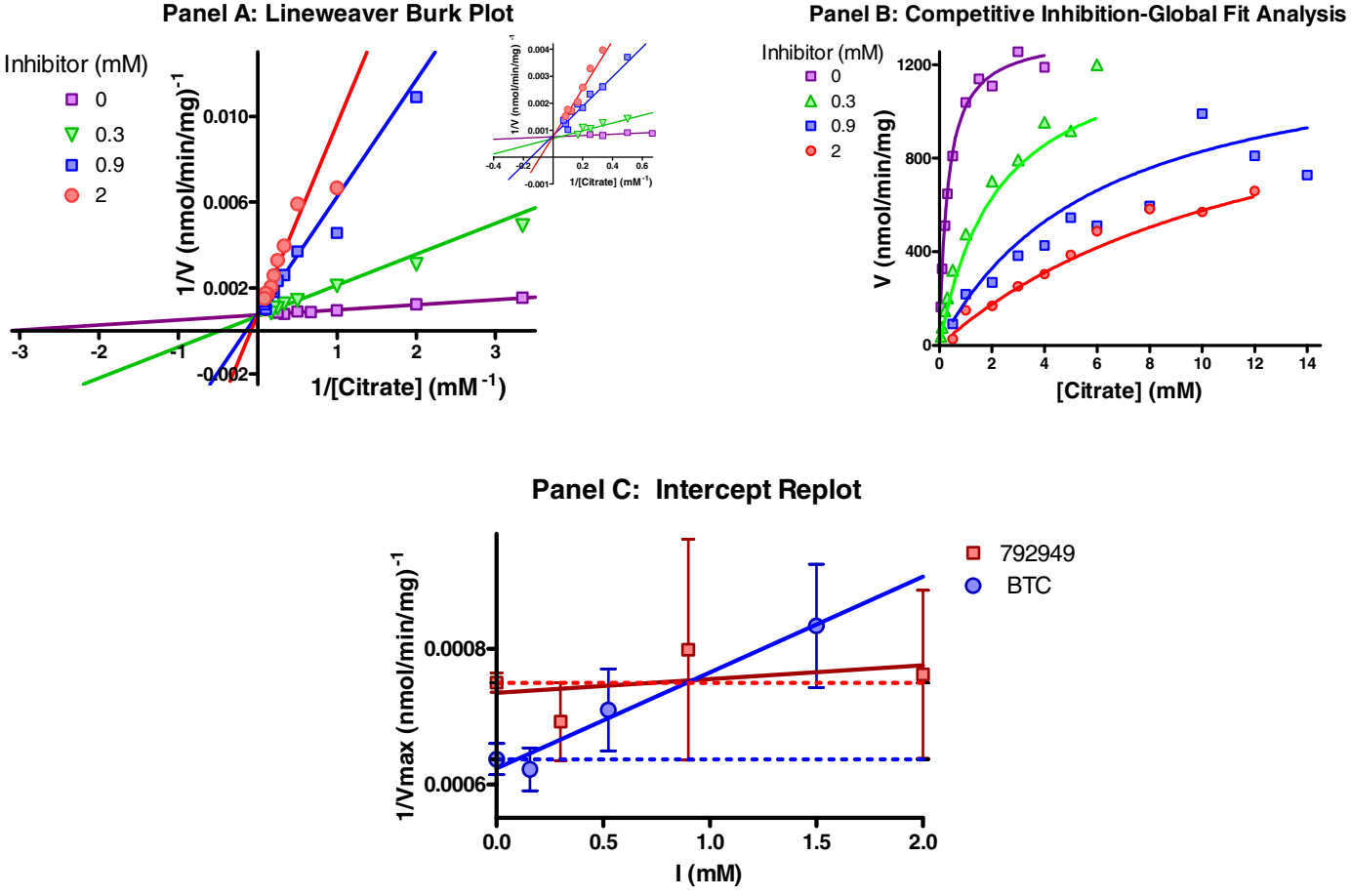

Fig. 6. Determination of kinetic mechanism and the competitive inhibition constant for ZINC compound 792949-mediated inhibition of the Cys-less CTP. A, Lineweaver-Burk plot depicting the effect of 792949 on the citrate transport activity. The citrate/citrate exchange (0.05–14 mM external/48 mM internal) was determined in the absence (purple line) and in the presence of 792949 (green line, 0.3 mM; blue line, 0.9 mM; and red line, 2 mM) as described under *Materials and Methods*. Nonlinear regression analysis of v-versus-[S] data was used to calculate V_{max} (apparent) and K_m (apparent) for each inhibitor concentration. These lines were then plotted on a double reciprocal plot. Inset shows the y-intercept ($1/V_{max}$) of each line. The V_{max} (apparent) does not change with increasing concentrations of the inhibitor 792949, whereas K_m (apparent) increases. B, global fit analysis of v-versus-[S] data (in the presence and absence of inhibitor) fitted simultaneously according to the full nonlinear expression for competitive inhibition. C, replot of $1/V_{max}$ (apparent) versus inhibitor (I) concentration. The slopes of the 792949 and the BTC best fit lines are $2.1 \pm 3.2 \times 10^{-5}$ and $14.2 \pm 1.8 \times 10^{-5}$, respectively. The dashed lines depict an ideal competitive inhibitor (i.e., 0 slope) using the V_{max} obtained in the absence of either 792949 (red dashed line) or BTC (blue dashed line). Note that the observed difference in $1/V_{max}$ in the absence of inhibitor reflects differences in assay conditions and protein preparations.

1. Upon reconstitution of the Cys-less CTP variant in liposomal vesicles [which we have demonstrated previously to display native-like functional properties (Xu et al., 2000)], BTC, the defining inhibitor of the CTP, functions as a mixed inhibitor with a strong competitive component (Fig. 2). Docking calculations conducted with BTC and our homology-modeled CTP structure (Fig. 3) indicate that although BTC can bind to both substrate binding sites 1 and 2, it displays a clear preference for the second binding site.
2. With the eight residues that were previously identified as forming the two substrate binding sites within the CTP, we observed that increases in the K_{ic} of each mutant for BTC, relative to the Cys-less control, generally parallel the observed increases in the K_m values of these mutants for citrate transport. This finding, in combination with our earlier finding that the k_{cat} value for each of these mutants is dramatically reduced, lends strong support to our contention that with these single-Cys CTP variants, the K_m for citrate transport approximates the K_d for citrate and therefore primarily reflects the affinity of the transporter for substrate.
3. Our results demonstrate the effectiveness of the application of DOCK-based high-throughput in silico screening to a homology-based transporter model in facilitating the discovery of novel competitive inhibitors. The best inhibitor that we identified (i.e., compound 792949) has a slightly higher affinity for the CTP than does BTC and is a purely competitive inhibitor. Most importantly, in contrast to BTC, it is of sufficient length that it is predicted to bind to both of the citrate binding sites simultaneously, which may result in a CTP that is locked in a single conformation.

Because the transporter binding sites contain a number of positively charged side-chains, it is not surprising that the identified inhibitors contain one or two carboxylates. BTC is a relatively small molecule, and its interactions are primarily with positively charged residues in the second of two previously identified substrate binding sites. It is interesting to note that 7 of the 10 newly identified inhibitors from the ZINC database also contain a sulfonamide group that is often acidic (Scior et al., 1997). Furthermore, many of these compounds are of significantly greater length than BTC, thus raising the possibility that they may be able to bind to residues in both citrate binding sites simultaneously.

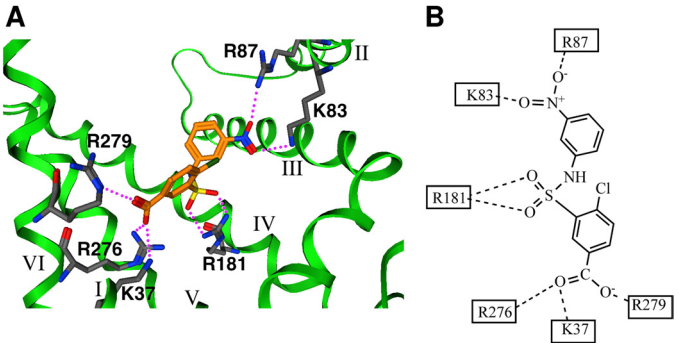

Fig. 7. Important binding interactions for the docked conformation of ZINC compound 792949 with the mitochondrial CTP model. Residues Lys83 and Arg87 are part of substrate site 1, and Lys37, Arg181, Arg276, and Arg279 are part of substrate site 2, as described previously (Ma et al., 2007). A, CTP backbone shown as a green ribbon, with transmembrane domains identified using Roman numerals, with interacting side-chains shown as stick structures colored by atom type, and 792949 shown as a stick structure with orange carbon atoms. Ion-pair and ionic hydrogen bond interactions are shown using magenta dotted lines. Portions of helices I and II have been removed for clarity. The inhibitor and important CTP side-chains are represented as stick structures: blue, nitrogen; red, oxygen; yellow, sulfur; green, chlorine; gray, CTP carbon; and orange, inhibitor carbon. B, schematic representation with ion-pair and ionic hydrogen bond interactions shown as dotted lines.

With the recent identification of two distinct citrate binding sites that reside within the hydrophilic transport pathway of the CTP in the cytoplasmic-facing conformation (Ma et al., 2007), a number of different kinetic mechanisms for transport can be proposed. One such mechanism would posit that two molecules of citrate are required to be bound before transport of the citrate bound at binding site 2 (the more interior binding site; see Fig. 1). However, such a model gives rise to nonhyperbolic velocity versus substrate concentration curves and parabolic Lineweaver-Burk curves, which are not seen in the wild-type (Xu et al., 2000), Cys-less, or other mutated forms of the transporter (Supplemental Fig. 1). Alternatively, one might suppose that in the presence of a citrate molecule bound at site 2, the binding of a second citrate molecule to site 1 might actually inhibit the transport process. This would give rise to substrate inhibition and a "checkmark" shape to the Lineweaver-Burk curve. There is no evidence of substrate inhibition even when citrate concentrations are greater than six times K_m. Thus, only mechanisms that bind and transport one citrate molecule at a time through one transport pathway/monomer should be further contemplated. The fact that cysteine substitution for each of the CTP binding site residues all give rise to transporters with highly elevated K_m values can best be explained by a sequential model in which citrate first binds to the outer binding site (site 1) with an equilibrium dissociation constant of K_{d1} (for the reaction Citrate · Site1 ↔ Citrate + Site1) and then to the inner binding site (site 2) with an equilibrium constant of K_{d2} (for the reaction Citrate · Site2 ↔ Citrate · Site1) to give an overall binding constant of $K_d = K_{d1} \cdot K_{d2}$. This implies that a citrate molecule bound at site 2 is not able to directly dissociate back to the external milieu (i.e., the cytosol). Viewed from a functional perspective, this model implies that 1) a single molecule of citrate moves sequentially from site 1 to site 2 but cannot physically contact all of the residues in these two sites simultaneously and 2) all eight residues that comprise binding sites 1 and 2 contribute in an essential manner to citrate binding before the transport event. For these binding site variants, where V_{max} is greatly reduced (Supplemental Fig. 1), K_m should approximate K_d. This assumption was shown to be substantially correct by the nearly linear relationship across all the cysteine variants between the change in the binding energy (ΔG) of the inhibitor BTC relative to that of the Cys-less control ($\Delta\Delta G$) and the log of the ratio of the K'_m of the variants to the K_m of the Cys-less control transporter (See Fig. 4). If K_m had a substantial contribution from k_{cat}, we would expect a great deal more scatter in this plot. The observation that six of the variants essentially lie on the best fit line strongly suggests that the K_m for citrate transport closely approximates the K_d for citrate binding. It should be pointed out that the K239C variant not only significantly lies to the right of the best fit line but is also the variant with the highest V_{max}, suggesting that for this mutant, K_m has a significant k_{cat} component. The unusually high BTC binding

constant for the R276C variant can be understood as this residue's having a more significant role in BTC binding than citrate binding. It is noteworthy that both of these residues reside within binding site 2, which modeling studies suggested to be the favored BTC binding site.

A number of different models for BTC binding can be proposed to explain how BTC, a molecule very similar in structure to citrate, causes mixed inhibition (Figs. 2, A and B, and 6C) rather than purely competitive inhibition, as has been assumed for more than 35 years (Robinson et al., 1971; Robinson et al., 1971a,b; Palmieri et al., 1972; Bisaccia et al., 1990). Although the competitive (and more pronounced) aspect of this inhibition is obviously due to BTC's structural similarity to citrate and the fact that its two binding sites overlap with the two citrate binding sites in the modeled cytosolic-facing conformation, the uncompetitive aspect of BTC inhibition may provide some clues about the mechanics of citrate transport. To understand the uncompetitive component of BTC inhibition, one may posit that BTC binds to site 1 when the transporter is in its alternative matrix-facing conformation (not modeled). BTC binding might stabilize the matrix-facing conformation and decrease the rate at which CTP progresses through its transport cycle. By interfering with the conformational cycling, V_{max} would decrease. We further posit that external citrate, perhaps because of its hydrophilicity, is not capable of binding to this matrix-facing conformation of site 1, as evidenced by the lack of substrate inhibition. It is noteworthy that this mechanism would hold true whether CTP functions as a monomer or a homodimer, an issue that is controversial (Palmieri et al., 1992; Kotaria et al., 1999; Bamber et al., 2007). This interference in the transport cycle could manifest itself either in the context of a single monomer or as part of a coordinated dimeric structure in which one protomer is in the cytosolic-facing conformation and the other is in the matrix-facing conformation. The presence of BTC in site 1 of the protomer in the matrix-facing conformation might limit the ability of the other protomer to change conformation.

From this analysis, strictly competitive inhibitors such as compound 792949 must only be capable of binding to CTP site 1 and/or site 2 in the cytosolic-facing conformation. Binding to other sites or site 1 in the matrix-facing conformation leads to an uncompetitive component in the inhibition pattern. In the case of 792949 itself, its lack of uncompetitive inhibition can be readily explained by the model whereby the molecule enters site 1, proceeds to site 2, and in contrast to citrate then binds to residues from both sites simultaneously.

In conclusion, these studies have provided important insight into the mechanism of the mitochondrial CTP and have led to the development of a physical model explaining its modes of interaction with BTC. In addition, using high-throughput in silico screening of the ZINC database with the homology-modeled CTP, we have discovered a novel inhibitor (i.e., compound 792949) that has a slightly higher affinity than BTC, is purely competitive, and is likely to span both substrate binding sites. This inhibitor may prove to be an effective conformational-stabilizing tool in our CTP structural studies.

Acknowledgments

We thank Austin Kirschner, John J. Irwin, and Brian K. Shoichet for helpful discussions.

References

Bamber L, Harding M, Monné M, Slotboom DJ, and Kunji ER (2007) The yeast mitochondrial ADP/ATP carrier functions as a monomer in mitochondrial membranes. *Proc Natl Acad Sci U S A* **104:**10830–10834.

Bisaccia F, De Palma A, Prezioso G, and Palmieri F (1990) Kinetic characterization of the reconstituted tricarboxylate carrier from rat liver mitochondria. *Biochim Biophys Acta* **1019:**250–256.

Cortés A, Cascante M, Cárdenas ML, and Cornish-Bowden A (2001) Relationships between inhibition constants, inhibitor concentrations for 50% inhibition and types of inhibition: new ways of analysing data. *Biochem J* **357:**263–268.

Greville GD (1969) Intracellular compartmentation and the citric acid cycle, in *Citric Acid Cycle Control and Compartmentation* (Lowenstein JM ed) pp 1–136, Marcel Dekker, NewYork.

Ihlenfeldt WD, Voigt JH, Bienfait B, Oellien F, and Nicklaus MC (2002) Enhanced CACTVS browser of the Open NCI Database. *J Chem Inf Comput Sci* **42:**46–57.

Irwin JJ and Shoichet BK (2005) ZINC—a free database of commercially available compounds for virtual screening. *J Chem Inf Model* **45:**177–182.

Kaplan RS and Pedersen PL (1985) Determination of microgram quantities of protein in the presence of milligram levels of lipid with amido black 10B. *Anal Biochem* **150:**97–104.

Kaplan RS, Mayor JA, Johnston N, and Oliveira DL (1990) Purification and characterization of the reconstitutively active tricarboxylate transporter from rat liver mitochondria. *J Biol Chem* **265:**13379–13385.

Kaplan RS, Mayor JA, Gremse DA, and Wood DO (1995) High level expression and characterization of the mitochondrial citrate transport protein from the yeast *Saccharomyces cerevisiae*. *J Biol Chem* **270:**4108–4114.

Kotaria R, Mayor JA, Walters DE, and Kaplan RS (1999) Oligomeric state of wild-type and cysteine-less yeast mitochondrial citrate transport proteins. *J Bioenerg Biomembr* **31:**543–549.

Ma C, Kotaria R, Mayor JA, Eriks LR, Dean AM, Walters DE, and Kaplan RS (2004) The mitochondrial citrate transport protein: probing the secondary structure of transmembrane domain III, identification of residues that likely comprise a portion of the citrate transport pathway, and development of a model for the putative TMDIII-TMDIII' interface. *J Biol Chem* **279:**1533–1540.

Ma C, Remani S, Sun J, Kotaria R, Mayor JA, Walters DE, and Kaplan RS (2007) Identification of the substrate binding sites within the yeast mitochondrial citrate transport protein. *J Biol Chem* **282:**17210–17220.

Palmieri F, Bisaccia F, Capobianco L, Dolce V, Iacobazzi V, Indiveri C, and Zara V (1992) Structural and functional properties of two mitochondrial transport proteins: the phosphate carrier and the oxoglutarate carrier, in *Molecular Mechanisms of Transport* (Quagliariello E and Palmieri F eds) pp 151–158, Elsevier, New York.

Palmieri F, Stipani I, Quagliariello E, and Klingenberg M (1972) Kinetic study of the tricarboxylate carrier in rat liver mitochondria. *Eur J Biochem* **26:**587–594.

Pebay-Peyroula E, Dahout-Gonzalez C, Kahn R, Trézéguet V, Lauquin GJ, and Brandolin G (2003) Structure of mitochondrial ADP/ATP carrier in complex with carboxyatractyloside. *Nature* **426:**39–44.

Robinson BH (1971) The role of the tricarboxylate transporting system in the production of phosphoenolpyruvate by ox liver mitochondria. *FEBS Lett* **16:**267–271.

Robinson BH, Williams GR, Halperin ML, and Leznoff CC (1971a) Factors affecting the kinetics and equilibrium of exchange reactions of the citrate-transporting system of rat liver mitochondria. *J Biol Chem* **246:**5280–5286.

Robinson BH, Williams GR, Halperin ML, and Leznoff CC (1971b) The sensitivity of the exchange reactions of tricarboxylate, 2-oxoglutarate and dicarboxylate transporting systems of rat liver mitochondria to inhibition by 2-pentylmalonate, p-iodobenzylmalonate, and benzene 1,2,3-tricarboxylate. *Eur J Biochem* **20:**65–71.

Scior T, Raddatz G, Figueroa R, Roth HJ, and Bisswanger HA (1997) Molecular modeling study on dapsone and sulfonamides comparing structures and properties with respect to anti-leprosy activity. *J Mol Model* **3:**332–337.

Shoichet BK, Kuntz ID, and Bodian DL (1992) Molecular docking using shape descriptors. *J Comput Chem* **13:**380–397.

Spencer AF and Lowenstein JM (1962) The supply of precursors for the synthesis of fatty acids. *J Biol Chem* **237:**3640–3648.

Srere PA and Bhaduri A (1962) Incorporation of radioactive citrate into fatty acids. *Biochim Biophys Acta* **59:**487–489.

Walters DE and Kaplan RS (2004) Homology-modeled structure of the yeast mitochondrial citrate transport protein. *Biophys J* **87:**907–911.

Watson JA and Lowenstein JM (1970) Citrate and the conversion of carbohydrate into fat. Fatty acid synthesis by a combination of cytoplasm and mitochondria. *J Biol Chem* **245:**5993–6002.

Xu Y, Mayor JA, Gremse D, Wood DO, and Kaplan RS (1995) High-yield bacterial expression, purification, and functional reconstitution of the tricarboxylate transport protein from rat liver mitochondria. *Biochem Biophys Res Commun* **207:**783–789.

Xu Y, Kakhniashvili DA, Gremse DA, Wood DO, Mayor JA, Walters DE, and Kaplan RS (2000) The yeast mitochondrial citrate transport protein. Probing the roles of cysteines, Arg(181), and Arg(189) in transporter function. *J Biol Chem* **275:**7117–7124.

Address correspondence to: Ronald S. Kaplan, Department of Biochemistry and Molecular Biology, Chicago Medical School, Rosalind Franklin University of Medicine and Science, North Chicago, IL 60064. E-mail: ronald.kaplan@rosalindfranklin.edu